Letter Vol. 6, No. 9 / September 2019 / Optica 1106

Megahertz x-ray microscopy at x-ray free-electron laser and synchrotron sources

Patrik Vagovič,[1,2,3,*] Tokushi Sato,[1,2] Ladislav Mikeš,[2] Grant Mills,[2] Rita Graceffa,[2] Frans Mattsson,[4] Pablo Villanueva-Perez,[4,1] Alexey Ershov,[5] Tomáš Faragó,[5] Jozef Uličný,[6] Henry Kirkwood,[2] Romain Letrun,[2] Rajmund Mokso,[4] Marie-Christine Zdora,[7,8,9] Margie P. Olbinado,[10] Alexander Rack,[10] Tilo Baumbach,[5] Joachim Schulz,[2] Alke Meents,[1] Henry N. Chapman,[1] and Adrian P. Mancuso[2,11]

[1]Center for Free-Electron Laser, Notkestraße 85, 22607 Hamburg, Germany
[2]European XFEL, Holzkoppel 4, 22869 Schenefeld, Germany
[3]Institute of Physics, Academy of Sciences of the Czech Republic v.v.i., Na Slovance 2, 182 21, Praha 8, Czech Republic
[4]Lund University, Sweden
[5]Institute for Photon Science and Synchrotron Radiation, Karlsruhe Institute of Technology (KIT), Herrmann-von-Helmholtz-Platz 1, 76344 Eggenstein-Leopoldshafen, Germany
[6]Faculty of Science, Department of Biophysics, P. J. Šafárik University, Jesenná 5, 04154 Košice, Slovakia
[7]Diamond Light Source, Harwell Science and Innovation Campus, Didcot, Oxfordshire OX11 0DE, UK
[8]Department of Physics & Astronomy, University College London, London, WC1E 6BT, UK
[9]Department of Physics & Astronomy, University of Southampton, Southampton SO17 1BJ, UK
[10]ESRF – The European Synchrotron, 71 Avenue des Martyrs, 38000 Grenoble, France
[11]Department of Chemistry and Physics, La Trobe Institute for Molecular Science, La Trobe University, Melbourne, Victoria 3086, Australia
*Corresponding author: patrik.vagovic@xfel.eu

Received 13 June 2019; revised 22 July 2019; accepted 26 July 2019 (Doc. ID 369962); published 23 August 2019

Modern emerging technologies, such as additive manufacturing, bioprinting, and new material production, require novel metrology tools to probe fundamental high-speed dynamics happening in such systems. Here we demonstrate the application of the megahertz (MHz) European X-ray Free-Electron Laser (EuXFEL) to image the fast stochastic processes induced by a laser on water-filled capillaries with micrometer-scale spatial resolution. The EuXFEL provides superior contrast and spatial resolution compared to equivalent state-of-the-art synchrotron experiments. This work opens up new possibilities for the characterization of MHz stochastic processes on the nanosecond to microsecond time scales with object velocities up to a few kilometers per second using XFEL sources.

https://doi.org/10.1364/OPTICA.6.001106

Hard x-ray beams are well suited for microscopic two-dimensional (2D) and three-dimensional (3D) imaging of samples not transparent to visible light due to their high penetration power. Over the last two decades, the field of x-ray imaging has developed considerably, mainly due to the availability of modern third-generation synchrotrons producing x rays of high brilliance [1]. These sources have provided access to the structural determination of specimens down to nanometer-scale resolutions. Exploiting the (partial) spatial coherence of synchrotron x-ray probes, several phase-sensitive techniques have been developed providing access to the electron density of specimens either via x-ray optical analyzers [2–4] or sophisticated algorithms [5,6]. While much attention has been paid to improving the spatial resolution of x-ray imaging to its limits, fewer resources have been used to explore the boundaries of the temporal domain. With the progress in the development of detectors over the last decade [7], fast radiography and tomography with kilohertz frame rates are available, allowing, for example, ∼100 tomograms per second [8,9]. Only relatively recently has the stroboscopic nature of synchrotrons been exploited. For example, imaging with synchronized or individual x-ray pulses applied to fast stochastic transient processes has been demonstrated [10–12]. Further advancement of ultrafast x-ray imaging could be introduced by megahertz (MHz) x-ray free-electron laser (XFEL) sources, where the high flux per pulse can reveal dynamics of stochastic processes with velocities up to the scale of several kilometers per second with submicron-scale resolutions with high sensitivity to projected densities. In this work, we exploit the unique properties of the first operational hard x-ray MHz XFEL source European XFEL (EuXFEL) and explore its possibilities for ultrafast x-ray microscopy with MHz sampling. The laser-induced dynamic processes in an open-ended glass capillary filled with water was used as a dynamic sample. We use this simple model system to show the advantages of microsecond temporal resolution, micrometer spatial resolution, and the improved signal-to-noise in the images all brought about by using a MHz repetition rate XFEL. We compare the results obtained at EuXFEL to that at European

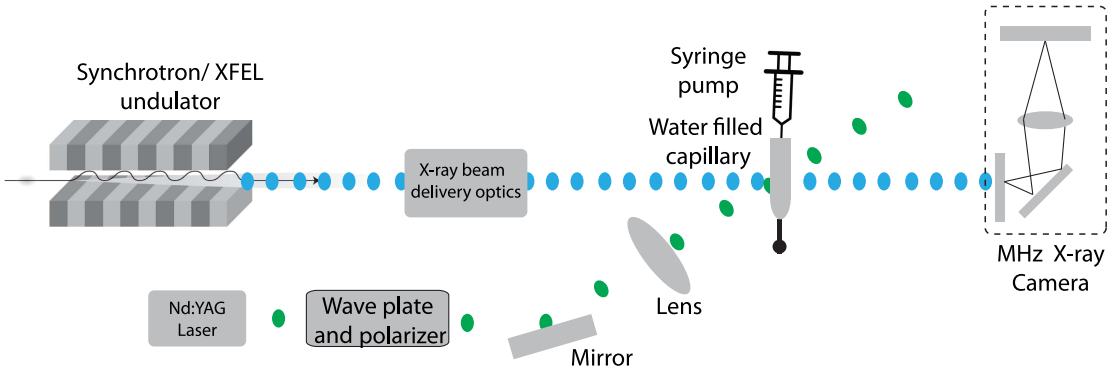

Fig. 1. Schematics of the time-resolved MHz x-ray microscopy of laser-induced dynamics in a water-filled glass capillary.

Synchrotron Radiation Facility (ESRF) ID19 beamline with the setup depicted in Fig. 1. The first results obtained at EuXFEL are already comparable to the state-of-the-art synchrotron performance [12] and are still subject to improvement. Further developments will allow for improving the spatial resolution beyond the reach of most brilliant synchrotron sources with potential acquisition of 3D MHz movies by employing x-ray multiprojection imaging [13].

It has been reported that liquid jets with velocities as high as 850 m/s can be generated by focusing a visible light laser into a capillary filled with water [14]. A jet based on this principle may be considered for needle-free drug-delivery injection or for sample delivery applications at MHz XFEL sources as a jet on demand, which can significantly minimize the sample usage. The characterization of the laser-induced jets and fluidics on the nanosecond to microsecond time scales is typically done by visible light microscopy. However, details on the microstructure are difficult or impossible to access with light microscopy due to the large refraction angle and strong multiple light scattering at the interfaces caused, for example, by microcavitations [15]. To explore the dynamics induced by the focused frequency-doubled Nd:YAG laser (Minilite II, Continuum) in the glass capillaries filled with water, we constructed conceptually similar time-resolved microscopy setups at the ID19 beamline at ESRF and at the Single Particles, Clusters and Biomolecules and Serial Femtosecond Crystallography (SPB/SFX) instrument of the EuXFEL using an indirect scintillator-based detector coupled to the MHz frame transfer CMOS camera SHIMADZU HPV-X2 schematically depicted in Fig. 1.

For the experiment at EuXFEL, we used the SPB/SFX instrument [16]. For the x-ray microscopy measurements, we reused the spent beam from the upstream interaction region and was outcoupled into air via a 180 μm thick diamond window. A photon energy of 9.3 keV was used, and the pulse train was filled with 128 x-ray pulses with a repetition rate of 1.128 MHz. The effective pixel size of the imaging system was 3.2 μm (see Supplement 1).

For the experiment at the ESRF synchrotron, we used the 16-bunch filling mode, providing a bunch separation of 176 ns; the MHz camera was recording every third frame with an interframe time of 530 ns. The harmonics of the undulator with central photon energy 32 keV were conditioned by a set of 1D compound refractive lenses to enhance the flux density at the detector. The effective pixel size of the imaging system was 8 μm (see Supplement 1).

Stable jetting conditions were achieved at ESRF, with an incident laser pulse energy of 2 mJ and approximately 0.05 total absorbency of the laser power in water mixed with Nile blue dye, resulting in approximately 100 μJ absorbed energy per pulse. This was enough to form the repeatable jet [Fig. 3(a)]. This result is consistent with previous reported results [14]. The measured water jet speed is 184 m/s, and the wall velocity of the laser cavity expanding wall reaches 272 m/s. The transformation of the meniscus into the jet during first frames is also clearly visible with clear detail. Due to limited time during the EuXFEL experiment, jetting conditions were not achieved. However, due to the high contrast achieved and high spatial resolution, the microstructure of the laser interaction with the sample is revealed with great detail (Fig. 2), which is not possible by visible light microscopy. To compare quantitatively the imaging performance for both experiments, we used a signal-to-noise ratio (SNR) analysis and power spectrum analysis. Detailed description about applied analysis is described in the supplementary document. As a result, the SNR analyzed for both ESRF and EuXFEL sequences show almost 2 times higher values for the maximum SNR from each analyzed sequence for EuXFEL with SNR = 10.69 and for ESRF with SNR = 6.19 [Figs. 3(b) and 3(d)]. A more objective comparison using spectral power [Fig. 3(c)] clearly indicates the superior performance of EuXFEL microscopy over ESRF. However, stronger fluctuation in the mean values and SNR are observed for XFEL data. This is a natural behavior of XFEL beams and is related to the origin of x-ray pulse generation using the self-amplified spontaneous emission (SASE) process. Such fluctuations are the reason for the lack of a procedure for correct data normalization, as every sequence and pulse has a different intensity distribution. Simple normalization of such data leads to image flickering and the increase of the standard deviation of the signal. Another contribution responsible for the increase of the standard deviation for the actual EuXFEL data is attributed to the high-frequency noise caused by the focusing kilobyte optics. To remove normalization artifacts and high-frequency noise for the EuXFEL data, we performed an adaptive high-pass filtering by subtracting a low-pass filtered (Gaussian convolution with the standard deviation $\sigma = 5$ pixels) image from its original version. This procedure significantly suppressed spatiotemporal image flickering. Using such image processing, we visualized the velocities of breaking glass reaching 35 m/s using flow analysis based on variational optical flow methods [17]. The computed velocities provide quantitative information about complex kinematics of the burst process

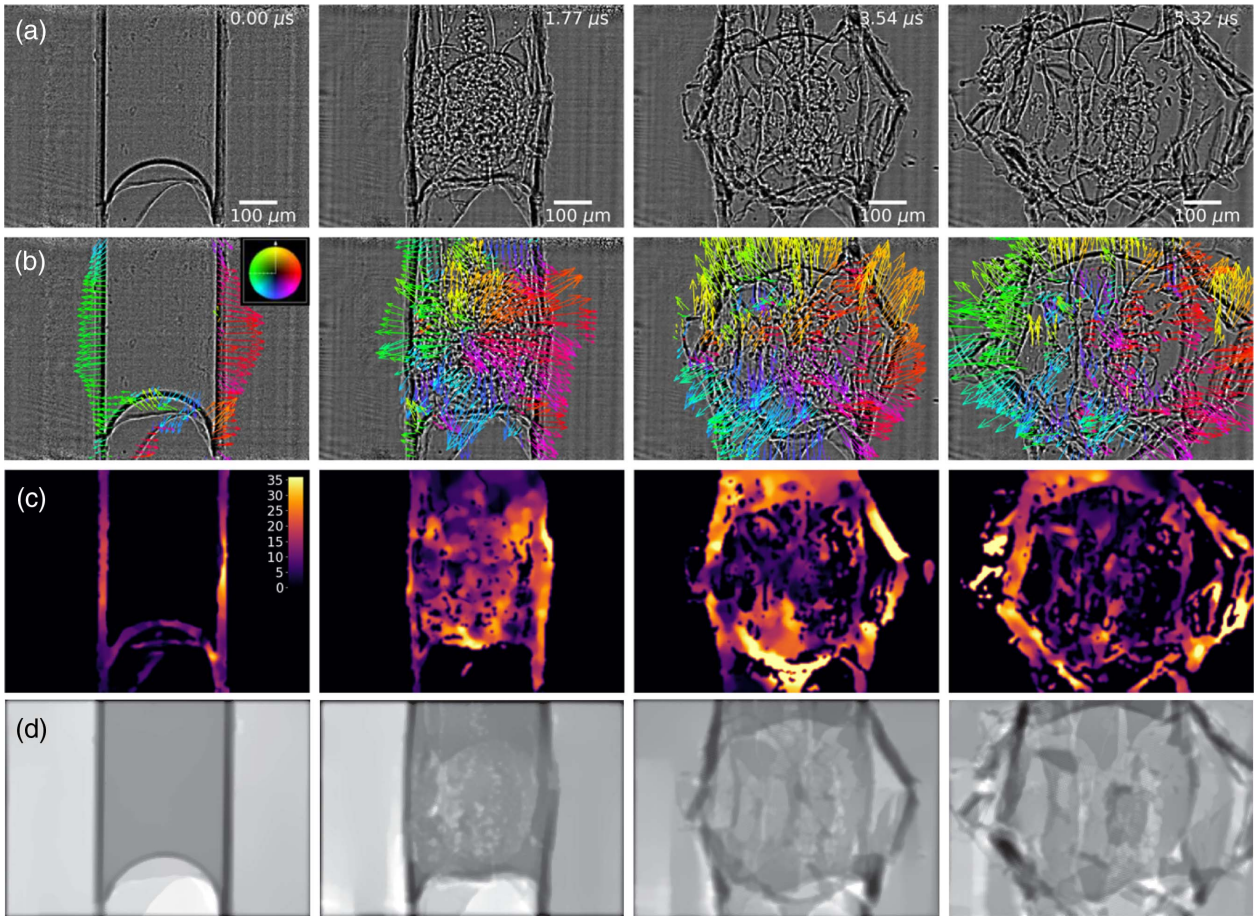

Fig. 2. Image sequence of laser-driven explosion of a capillary filled with water imaged at EuXFEL. Sequence (a) is the result of high-pass adaptive filtering to remove the high-frequency noise and image flickering; sequences (b) and (c) are the result of optical flow analysis [17] shown as a directional vector for the movement of debris (b) and the velocity maps (c) (see Visualization 1). The phase retrieval of the corresponding sequence (d) is performed using an ADMM-CTF algorithm [18].

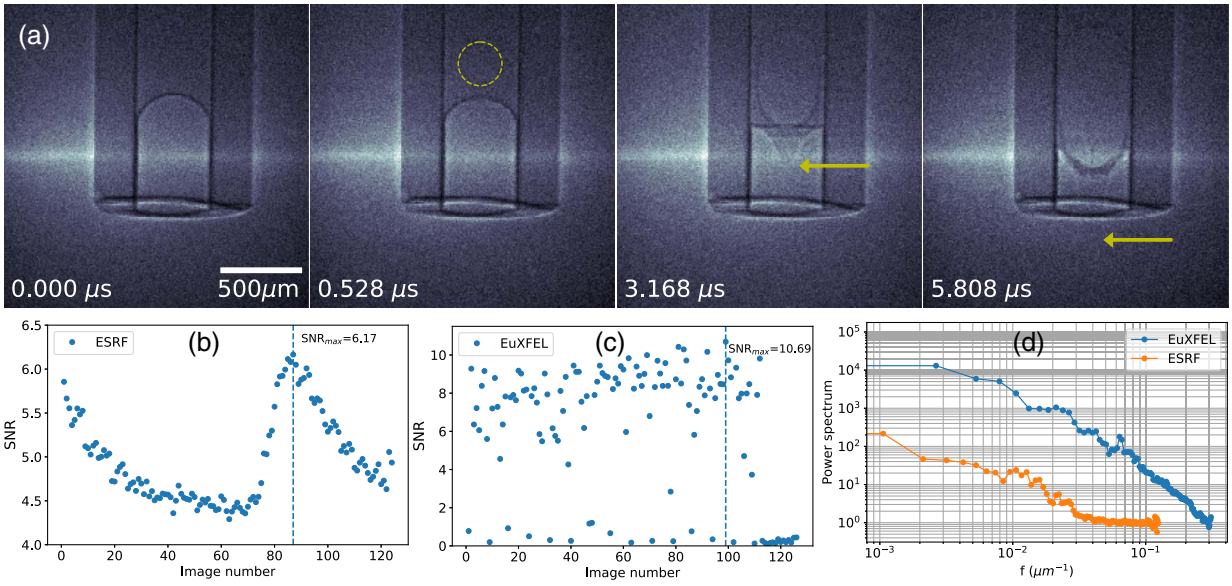

Fig. 3. (a) Image sequence of a water jet generated by absorbed power (~2 mJ pulse energy) of a focused visible-light laser inside the glass capillary (see Visualization 2) imaged at the ESRF synchrotron. The circle on the second frame shows the laser-induced cavitation with radius of 144 μm indicating an initial velocity of 272 m/s of the expanding wall. The arrows on the third and fourth frame indicate the tip of the water jet reaching a velocity of 184 m/s. The signal to noise analysis for (b) ESRF and (c) EuXFEL and (d) power spectrum curves shows superior image performance of EuXFEL data. For detailed description of SNR (b) and (c) and power spectrum analysis (d), see Supplement 1 for supporting content.

(see Supplement 1 for supporting content). The high spatial coherence of XFEL data allowed us to apply a contrast-transfer function (CTF)-based phase-retrieval method utilizing the alternating direction method of multipliers (ADMM) [18]. The high spatial coherence of XFEL data allowed us to apply a contrast-transfer function (CTF)-based phase-retrieval method utilizing the alternating direction method of multipliers (ADMM) [18], shown in Fig. 2(d). Here the data were first normalized using a set of empty beam sequences; then the ADMM-CTF phase-retrieval algorithm was applied. High-frequency noise introduced by this process was removed by nonlocal-means denoising [19]. ADMM-CTF phase retrieval of the synchrotron data failed to provide meaningful phase reconstruction, which is attributed to the weak signal.

In conclusion, we have successfully demonstrated x-ray microscopy sampled at greater than 1 MHz at EuXFEL, and with the full performance of EuXFEL, maximum frame-rate of 4.5 MHz will be achievable. Our model system shows a significant improvement in the contrast of the data obtained at EuXFEL compared to data obtained at ESRF. This is due to the much higher photon flux per pulse as well as the much higher spatial coherence at EuXFEL. Such performance at EuXFEL additionally allowed for a 2.5-fold increase in the spatial resolution and a significant improvement in power spectrum over the entire range of frequencies, which enabled us to apply a single-distance phase-retrieval algorithm. This study opens up new perspectives for imaging, especially of irreversible stochastic processes not accessible via visible light imaging or with less intense x-ray sources. At hard x-ray MHz rate XFEL facilities, this method enables the observation of stochastic object motions at high velocities on the order of meters per second to several kilometers per second. High flux per pulse at EuXFEL will enable 3D MHz rate microscopy by employing beam splitters, which is the scope of our future development.

Funding. Bundesministerium für Bildung und Forschung (BMBF) (05K18XXA); Vetenskapsrådet (VR) (2017-06719).

Acknowledgment. We acknowledge Klaus Giewekemeyer, Luis Morillo Lopez, Cedric Michel Signe Takem, Alexis Legrand, Bradley Manning, and Nadja Reimers for technical support during preparation of the EuXFEL experiment. Beamtime was granted at ESRF beamline ID19 in the frame of proposal MI-1267.

See Supplement 1 for supporting content.

REFERENCES

1. C. Kunz, J. Phys. Condens. Matter **13**, 7499 (2001).
2. U. Bonse and M. Hart, Appl. Phys. Lett. **6**, 155 (1965).
3. D. Chapman, W. Thomlinson, R. E. Johnston, D. Washburn, E. Pisano, N. Gmür, Z. Zhong, R. Menk, F. Arfelli, and D. Sayers, Phys. Med. Biol. **42**, 2015 (1997).
4. C. David, B. Nöhammer, H. H. Solak, and E. Ziegler, Appl. Phys. Lett. **81**, 3287 (2002).
5. D. Paganin, S. C. Mayo, T. E. Gureyev, P. R. Miller, and S. W. Wilkins, J. Microsc. **206**, 33 (2002).
6. J. M. Rodenburg and H. M. L. Faulkner, Appl. Phys. Lett. **85**, 4795 (2004).
7. T. Hatsui and H. Graafsma, IUCrJ **2**, 371 (2015).
8. R. Mokso, C. M. Schlepütz, G. Theidel, H. Billich, E. Schmid, T. Celcer, G. Mikuljan, L. Sala, F. Marone, N. Schlumpf, and M. Stampanoni, J. Synchrotron Radiat. **24**, 1250 (2017).
9. W. Yashiro, D. Noda, and K. Kajiwara, Appl. Phys. Express **10**, 052501 (2017).
10. K. Fezzaa and Y. Wang, Phys. Rev. Lett. **100**, 104501 (2008).
11. M. P. Olbinado, X. Just, J.-L. Gelet, P. Lhuissier, M. Scheel, P. Vagovic, T. Sato, R. Graceffa, J. Schulz, A. Mancuso, J. Morse, and A. Rack, Opt. Express **25**, 13857 (2017).
12. N. D. Parab, C. Zhao, R. Cunningham, L. I. Escano, K. Fezzaa, W. Everhart, A. D. Rollett, L. Chen, and T. Sun, J. Synchrotron Radiat. **25**, 1467 (2018).
13. P. Villanueva-Perez, B. Pedrini, R. Mokso, P. Vagovic, V. A. Guzenko, S. J. Leake, P. R. Willmott, P. Oberta, C. David, H. N. Chapman, and M. Stampanoni, Optica **5**, 1521 (2018).
14. Y. Tagawa, N. Oudalov, C. W. Visser, I. R. Peters, D. van der Meer, C. Sun, A. Prosperetti, and D. Lohse, Phys. Rev. X **2**, 031002 (2012).
15. D. Hudgins and R. S. Abhari, Phys. Rev. E **99**, 031102 (2019).
16. A. P. Mancuso, A. Aquila, L. Batchelor, R. J. Bean, J. Bielecki, G. Borchers, K. Doerner, K. Giewekemeyer, R. Graceffa, O. D. Kelsey, Y. Kim, H. J. Kirkwood, A. Legrand, R. Letrun, B. Manning, L. L. Morillo, M. Messerschmidt, G. Mills, S. Raabe, N. Reimers, A. Round, T. Sato, J. Schulz, C. S. Takem, M. Sikorski, S. Stern, P. Thute, P. Vagovič, B. Weinhausen, and T. Tschentscher, J. Synchrotron Radiat. **26**, 660 (2019).
17. A. Myagotin, A. Ershov, L. Helfen, R. Verdejo, A. Belyaev, and T. Baumbach, J. Synchrotron Radiat. **19**, 483 (2012).
18. P. Villanueva-Perez, F. Arcadu, P. Cloetens, and M. Stampanoni, Opt. Lett. **42**, 1133 (2017).
19. A. Buades, B. Coll, and J.-M. Morel, Image Processing On Line **1**, 208 (2011).